Journal of the Korean Astronomical Society
50: 79 ∼ 92, 2017 June

https://doi.org/10.5303/JKAS.2017.50.3.79
pISSN: 1225-4614 · eISSN: 2288-890X
http://jkas.kas.org

BVI Photometric Study of the Old Open Cluster Ruprecht 6

Sang Chul Kim[1,2,3], Jaemann Kyeong[1], Hong Soo Park[1,2,3], Ilseung Han[1,4], Joon Hyeop Lee[1,2], Dae-Sik Moon[5], Youngdae Lee[1], and Seongjae Kim[1,4]

[1]Korea Astronomy and Space Science Institute, 776 Daedukdae-ro, Yuseong-gu, Daejeon 34055, Korea , sckim, jman, hspark, jhl, ylee@kasi.re.kr
[2]Korea University of Science and Technology (UST), 217 Gajeong-ro, Yuseong-gu, Daejeon 34113, Korea
[3]Visiting Astronomer, Cerro Tololo Inter-American Observatory, National Optical Astronomy Observatory
[4]Kyungpook National University, 80 Daehakro, Buk-gu, Daegu 41566, Korea; ihan@knu.ac.kr, ksj6283@naver.com
[5]Department of Astronomy and Astrophysics, University of Toronto, Toronto, ON M5S 3H4, Canada
moon@astro.utoronto.ca

Received May 4, 2017; accepted June 8, 2017

Abstract: We present a BVI optical photometric study of the old open cluster Ruprecht 6 using the data obtained with the SMARTS 1.0 m telescope at the CTIO, Chile. Its color-magnitude diagrams show the clear existence of the main-sequence stars, whose turn-off point is located around $V \approx 18.45$ mag and $B-V \approx 0.85$ mag. Three red clump (RC) stars are identified at $V = 16.00$ mag, $I = 14.41$ mag and $B-V = 1.35$ mag. From the mean K_s-band magnitude of RC stars ($K_s = 12.39 \pm 0.21$ mag) in Ruprecht 6 from 2MASS photometry and the known absolute magnitudes of the RC stars ($M_{K_S} = -1.595 \pm 0.025$ mag), we obtain the distance modulus to Ruprecht 6 of $(m-M)_0 = 13.84 \pm 0.21$ mag ($d = 5.86 \pm 0.60$ kpc). From the $(J-K_s)$ and $(B-V)$ colors of the RC stars, comparison of the $(B-V)$ and $(V-I)$ colors of the bright stars in Ruprecht 6 with those of the intrinsic colors of dwarf and giant stars, and the PARSEC isochrone fittings, we derive the reddening values of $E(B-V) = 0.42$ mag and $E(V-I) = 0.60$ mag. Using the PARSEC isochrone fittings onto the color-magnitude diagrams, we estimate the age and metallicity to be: $\log(t) = 9.50 \pm 0.10$ ($t = 3.16 \pm 0.82$ Gyr) and [Fe/H] $= -0.42 \pm 0.04$ dex. We present the Galactocentric radial metallicity gradient analysis for old (age > 1 Gyr) open clusters of the Dias et al. catalog, which likely follow a single relation of [Fe/H] $= (-0.034 \pm 0.007) R_{\rm GC} + (0.190 \pm 0.080)$ (rms $=$ 0.201) for the whole radial range or a dual relation of [Fe/H] $= (-0.077 \pm 0.017) R_{\rm GC} + (0.609 \pm 0.161)$ (rms $= 0.152$) and constant ([Fe/H] ~ -0.3 dex) value, inside and outside of $R_{\rm GC} \sim 12$ kpc, respectively. The metallicity and Galactocentric radius (13.28 ± 0.54 kpc) of Ruprecht 6 obtained in this study seem to be consistent with both of the relations.

Key words: open clusters and associations: individual (Ruprecht 6) — Galaxy: disk — Galaxy: stellar content — Galaxy: structure — Hertzsprung-Russell and color-magnitude diagrams — telescopes: CTIO 1.0 m

1. Introduction

The Galactocentric radial metallicity gradient in the disk of the Milky Way (MW) has been studied for a long time (e.g., Twarog et al. 1997; Park & Lee 1999; Chen et al. 2003; Tadross 2003; Kim 2006; Carraro et al. 2007; Paunzen et al. 2010; Netopil et al. 2016; Cantat-Gaudin et al. 2016; Jacobson et al. 2016; Tissera et al. 2016), for which open clusters (OCs) have been under intense studies, alongside with Cepheids (Andrievsky et al. 2004; Cescutti et al. 2007), globular clusters (Yong et al. 2008), red clump (RC) stars (Önal Taş et al. 2016), planetary nebulae (Stanghellini, & Haywood 2010), H II regions (Rudolph et al. 2006; Fernández-Martín et al. 2017), field stars (Xiang et al. 2015), etc. The disk metallicity gradient can give information on the disk formation processes, star formation processes, and chemical evolution of the spiral galaxies (Tissera et al. 2016). One notable recent result is that of Anders et al. (2017), who have claimed the slopes of the Galactic radial metallicity gradient to be $\simeq -0.066$ dex kpc^{-1} for the age range of $1-4$ Gyr and $\simeq -0.03$ dex kpc^{-1} for $6-10$ Gyr, using 418 red giant stars observed by CoRoT-APOGEE for $6 < R_{\rm GC} \lesssim 13$ kpc and $\mid Z_{gal} \mid < 0.3$ kpc (where $R_{\rm GC}$ is the Galactocentric distance and Z_{gal} is the vertical distance from the Galactic plane).

OCs, especially the old ones, are a good laboratory for verifying stellar evolution theories. They are also good tracers of the star formation and evolutionary history of the Galactic disk. While Lyngå (1987) published data for over 1200 OCs, the observed number of OCs, including candidates, has increased to 2167 in the latest version (3.5; 2016 January 28) of Dias et al. (2002) (hereafter DAML02) catalog.[1] Among the 2167 objects in the DAML02 OC catalog, only 298 (13.8%) have metallicity estimates (Oliveira et al. 2013; Krisciunas et al. 2015), while 703 (32.4%) have radial velocity estimates, 2013 (92.9%) have age estimates, 2025 (93.4%) have reddening estimates, 2040 (94.1%) have distance

Corresponding author: S. C. Kim

[1]http://www.wilton.unifei.edu.br/ocdb

Table 1
Basic data of the open cluster Ruprecht 6

Parameter	Ruprecht 6	Reference
Other name	C 0653-132	SIMBAD
δ_{J2000}, α_{J2000}	$06^h\ 56^m\ 06^s$, $-13^\circ\ 15'\ 00''$	Hasegawa et al. (2008)
l,b	$225.^\circ28$, $-4.^\circ98$	Hasegawa et al. (2008)
Reddening, $E(B-V)$	0.42 mag	This study
Reddening, $E(V-I)$	0.60 mag	This study
Distance modulus, $(m-M)_0$	13.84 ± 0.21 mag	This study
Distance, d	5.86 ± 0.60 kpc	This study
Galactocentric distance, $R_{\rm GC}$	13.28 ± 0.54 kpc	This study
Metallicity, [Fe/H]	-0.42 ± 0.04 dex	This study
Age, t	3.16 ± 0.82 Gyr ($\log t = 9.50 \pm 0.10$)	This study
Trumpler type	III 1 p	Dias et al. (2002)

estimates, and 2104 (97.1%) have proper motion estimates. Kharchenko et al. (2013) presented MW object catalog for 3006 objects including 2808 OCs, 147 globular clusters, and 51 associations, almost complete up to 1.8 kpc from the Sun, where only 386 out of 3006 have metallicity values. Considering the estimated total number of MW OCs ($\sim 100\,000$; Piskunov et al. (2006); Tadross (2011)), more surveys and detailed photometric and spectroscopic studies on individual clusters would be fruitful.

Ruprecht 6 (Ruprecht 1966) is an old OC, located in the constellation of Canis Major and at very large distance ($\sim 13.28 \pm 0.54$ kpc; see Table 1 above) from the Galactic center. It is small and considered a poor OC, meaning it contains few member stars. This could be the reason why there have been few studies on the cluster. Hasegawa et al. (2008), which seems to be the only previous observational study on this cluster, used the 65-cm telescope, AP8 1024 px CCD, and BVI filters at Gunma Astronomical Observatory (FoV = $10.3' \times 10.3'$) to study 36 old OCs, and included Ruprecht 6 in their study. They obtained some physical parameters for Ruprecht 6 from Padova isochrone fitting : age = 3.2 Gyr ($\log t = 9.50$), $Z = 0.008$ ([Fe/H] = -0.41), $E(V-I) = 0.60$ mag, and $(m-M)_0 = 14.43$ ($d = 7.7$ kpc), and these values are enlisted in the DAML02 catalog. Some basic physical parameters are summarized in Table 1. The last parameter in Table 1 presents the Trumpler class of Ruprecht 6 to be III 1 p, which means, respectively, (i) Ruprecht 6 is detached and shows no noticeable concentration, (ii) most stars in the cluster are of nearly the same apparent brightness, and (iii) it is poor, containing less than 50 stars (as observed by Trumpler 1930; Dias et al. 2002).

In this study, using the BVI optical imaging data obtained at the CTIO 1.0 m telescope, we present the photometric analysis and physical parameters of the OC Ruprecht 6. Section 2 describes the observations and data reduction processes. Section 3 presents the results in this study: cluster center position, color-magnitude diagrams, reddening and distance estimations, and PARSEC isochrone fitting results. In Sections 4 and 5, we discuss the Galactocentric metallicity distribution and summarize our results, respectively.

2. OBSERVATIONS AND DATA REDUCTION

Observations have been done using the Small and Moderate Aperture Research Telescope System (SMARTS) 1.0 m telescope and Y4KCam CCD at the Cerro-Tololo Inter-American Observatory (CTIO, Chile) on 2010 December 13 (UT). The Y4KCam CCD, made at the Ohio State University, is composed of 4104×4104 pixels (each 15 μm, $\sim 0.289''$ pixel^{-1}) at the Cassegrain focus of the telescope. Its effective size becomes 4064×4064 pixels ($19.57' \times 19.57'$) after excluding the 40 pixel wide gaps from the horizontal and vertical centers separating the CCD into four quadrants and reading out the pixel values.[2]

For the OC Ruprecht 6, we have obtained three 1200 sec, three 900 sec, and two 800 sec images for B, V, and I filters, respectively, under $1.5''$ median seeing conditions. The final images are average combined for each filter. Figure 1 displays the combined grey-scale image of three V-band frames for the OC Ruprecht 6, where red circles show the region of Ruprecht 6 with radius of $2'$.

The raw observation data have been processed with the IRAF[3]/CCDRED package applying standard procedures – that is, the overscan correction, bias correction, and the twilight sky flattening have been made. Since interference patterns are seen in the I-band images, we made an I-band supersky image using all the I-band images obtained on the same night and performed a second flattening. In addition, because of the large format of the detector and the slow speed of the shutter, the shutter shading correction is applied. The IRAF script (`y4kshut.cl`) given at the CTIO homepage is used for the correction.

Photometry was performed using the DAOPHOT II/ALLSTAR stand-alone package after separating the CCD quadrants to treat them as four separate CCD chips (Stetson 1990). This is because each chip has a

[2] `http://www.astronomy.ohio-state.edu/Y4KCam/detector`
[3] IRAF is distributed by the National Optical Astronomy Observatory, which is operated by the Association of Universities for Research in Astronomy (AURA) under a cooperative agreement with the National Science Foundation.

different gain and readout noise. Due to the large field of view, we adopt the quadratic variable point spread function. Aperture corrections were obtained with $20-30$ isolated, bright, and unsaturated stars in each CCD quadrant. Figure 2 shows the error distribution of the BVI photometry results. The photometric errors typically attain 0.1 mag at $B \approx 22.7$ mag, $V \approx 22.4$ mag and $I \approx 21.2$ mag (Kim et al. 2009), indicating the object signal is ten times above the background.

Four Landolt (1992, 2007, 2009) standard star fields (PG0231+051, LB1735, LSS982, Rubin 149) were observed during the four nights of the observing run (2010 December $11-14$, UT) to obtain the standardization equations for this run and to convert the instrumental magnitudes to the standard magnitudes. The transformation equations are

$$\begin{aligned} B &= b - 0.285(\pm0.009)\, X_b - 0.127(\pm0.005)(B-V) \\ &\quad -1.903(\pm0.013) \\ V &= v - 0.157(\pm0.007)\, X_v + 0.027(\pm0.004)(B-V) \\ &\quad -1.693(\pm0.011) \\ I &= i - 0.056(\pm0.007)\, X_i + 0.019(\pm0.003)(V-I) \\ &\quad -2.712(\pm0.010) \end{aligned}$$

where lower case and upper case letters represent instrumental and standard magnitudes, respectively, and X is the airmass for each filter. We also have obtained the secondary extinction coefficient ($k_{2B} = -0.052 \pm 0.016$) as a free parameter. Including the secondary extinction coefficient, however, caused the errors of other parameters to increase and the overall residual remained at the same value (0.037). So we decided not to adopt k_{2B} but follow the simple solution. Figure 3 (a), (b), and (c) show the standardization residuals for the magnitude differences, where the rms of the fits are $\Delta B = 0.037$, $\Delta V = 0.030$, $\Delta I = 0.029$. Figure 3 (d) and (e) show the standardization residuals for the color differences, where the rms of the fits are $\Delta(B-V) = 0.017$, and $\Delta(V-I) = 0.019$. Astrometry was done using the routines provided in astrometry.net (Lang et al. 2010).

The total number of stars with photometry is 5570, while in the region of Ruprecht 6 with radius $< 2'$, the number is 296. Table 2 lists the photometry of 92 stars of Ruprecht 6 with $V < 19$ mag.

3. Results

3.1. Cluster Center and Size

For the center coordinates of the OC Ruprecht 6, Hasegawa et al. (2008) presents $\alpha_{J2000} = 06^h\ 56^m\ 06^s$, $\delta_{J2000} = -13^\circ\ 15'\ 00''$, which we adopt in this study. While Dias et al. (2002) (Version 3.5, 2016 January 28) lists $\alpha_{J2000} = 06^h\ 56^m\ 00^s$, $\delta_{J2000} = -13^\circ\ 17'\ 00''$ and SIMBAD gives $\alpha_{J2000} = 06^h\ 55^m\ 55.2^s$, $\delta_{J2000} = -13^\circ\ 16'\ 48''$, both of these values result in poor identifications of the cluster center. The coordinates given by Hasegawa et al. (2008) point to the cluster center more accurately as seen in Figure 1.

Using the bright stars ($V \leq 20$ mag) with the cluster center fixed as above, we plotted the radial number density profile with the bin size of $0.5'$ in Figure 4. We determined the radius of Ruprecht 6 to be $2.0'$, in which radius most of the member stars are located.

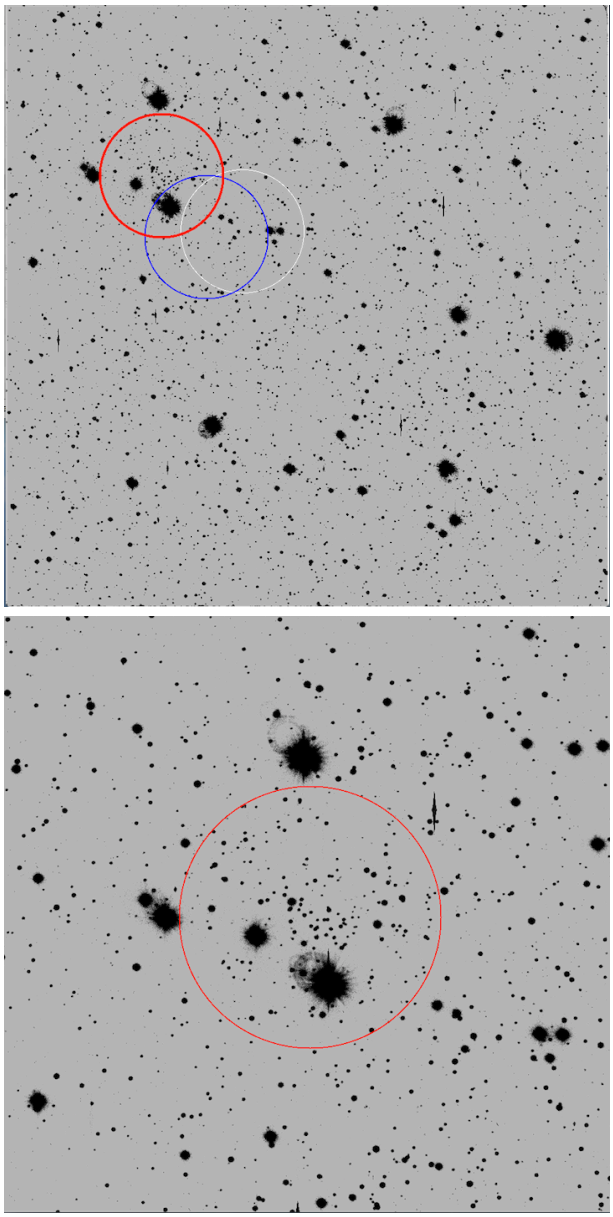

Figure 1. V-band grey-scale images of the open cluster Ruprecht 6. North is at the top and east is to the left. *Upper panel:* Y4KCam CCD image of the OC Ruprecht 6. The field-of-view of the image is $19.57' \times 19.57'$ (4064×4064 pixels). The thick red circle shows the region of Ruprecht 6 with radius of $2'$, centered on the coordinates of $\alpha_{J2000} = 06^h\ 56^m\ 06^s$ and $\delta_{J2000} = -13^\circ\ 15'\ 00''$ from Hasegawa et al. (2008), which is adopted in this study. Blue and white circles show the regions of radius of $2'$ centered on the coordinates of Dias et al. (2002) and SIMBAD, respectively. *Lower panel:* Zoomed-in image of the region of Ruprecht 6. Red circle shows the region of Ruprecht 6 with radius of $2'$(the same as in the upper panel) and the field-of-view of the image is $\sim 9' \times 9'$.

Table 2
Photometry data of bright stars with $V < 19$ mag in Ruprecht 6

ID	R.A. (J2000) hh:mm:ss	Dec. (J2000) dd:mm:ss	B	$\sigma(B)$	V	$\sigma(V)$	I	$\sigma(I)$	χ	sharpness
1	06:55:58.41	−13:15:02.73	20.25	0.012	18.99	0.005	17.46	0.006	1.010	−0.108
2	06:55:58.57	−13:15:20.15	19.97	0.009	18.95	0.006	17.68	0.011	1.312	0.176
3	06:55:59.86	−13:14:29.15	20.07	0.012	18.97	0.005	17.59	0.011	1.062	0.002
4	06:55:59.96	−13:15:59.53	20.11	0.010	18.80	0.005	17.37	0.005	1.004	−0.061
5	06:55:59.97	−13:15:13.03	19.00	0.006	17.91	0.003	16.62	0.008	1.032	−0.041
6	06:56:00.08	−13:15:17.20	20.15	0.019	18.75	0.005	17.18	0.005	1.180	0.122
7	06:56:00.13	−13:14:44.95	19.22	0.008	18.21	0.004	16.97	0.005	0.704	0.036
8	06:56:00.20	−13:14:42.57	16.64	0.002	15.71	0.002	14.62	0.004	1.335	−0.092
9	06:56:00.32	−13:15:08.39	19.65	0.006	18.75	0.006	17.56	0.008	1.198	0.170
10	06:56:00.51	−13:15:12.44	19.95	0.009	18.60	0.005	17.11	0.005	1.084	−0.091
11	06:56:00.61	−13:14:30.98	19.34	0.006	18.50	0.005	17.40	0.015	1.152	−0.034
12	06:56:00.98	−13:14:15.08	19.36	0.006	18.51	0.004	17.40	0.006	1.071	−0.012
13	06:56:01.08	−13:14:28.63	18.47	0.004	17.59	0.006	16.40	0.005	1.184	0.000
14	06:56:01.19	−13:13:53.88	19.29	0.007	18.45	0.006	17.39	0.006	1.242	0.000
15	06:56:01.21	−13:14:02.25	18.27	0.004	17.37	0.003	16.17	0.005	1.275	−0.082
16	06:56:01.47	−13:15:20.49	18.71	0.004	17.88	0.003	16.84	0.006	1.181	−0.049
17	06:56:01.65	−13:14:46.83	19.85	0.009	18.96	0.007	17.79	0.013	1.495	0.382
18	06:56:02.10	−13:15:55.44	18.96	0.004	18.15	0.003	17.09	0.005	1.008	−0.014
19	06:56:02.11	−13:16:43.81	17.84	0.003	17.02	0.002	16.04	0.004	1.110	0.049
20	06:56:02.26	−13:16:00.20	19.88	0.010	18.60	0.005	17.19	0.006	1.120	−0.092
21	06:56:02.41	−13:14:17.13	17.09	0.002	16.17	0.002	15.14	0.003	1.198	−0.050
22	06:56:03.23	−13:15:15.03	20.38	0.013	18.89	0.005	17.17	0.007	1.200	−0.092
23	06:56:03.85	−13:15:02.43	19.38	0.006	18.51	0.004	17.41	0.007	1.073	0.010
24	06:56:03.99	−13:15:28.30	18.79	0.008	17.95	0.009	16.77	0.007	1.288	0.172
25	06:56:04.02	−13:16:35.93	19.78	0.008	18.70	0.004	17.44	0.006	1.026	0.045
26	06:56:04.04	−13:15:08.75	18.86	0.005	17.99	0.003	16.83	0.005	1.175	−0.025
27	06:56:04.34	−13:15:24.36	20.15	0.012	18.70	0.005	16.89	0.005	1.165	0.016
28	06:56:04.46	−13:15:18.99	19.32	0.006	18.25	0.004	17.00	0.004	1.022	−0.018
29	06:56:04.67	−13:15:10.95	19.59	0.059	18.70	0.027	17.48	0.020	1.059	0.008
30	06:56:04.77	−13:14:22.56	19.60	0.007	18.36	0.004	16.95	0.005	1.069	−0.072
31	06:56:04.79	−13:14:53.61	18.05	0.003	17.21	0.002	16.10	0.004	1.152	−0.025
32	06:56:04.86	−13:15:02.45	19.55	0.007	18.68	0.005	17.55	0.007	1.071	0.006
33	06:56:04.94	−13:13:34.16	18.45	0.004	17.29	0.003	15.98	0.003	1.111	−0.037
34	06:56:04.96	−13:15:16.51	19.15	0.006	18.20	0.004	17.01	0.005	1.147	0.014
35	06:56:05.07	−13:15:02.69	19.58	0.007	18.71	0.005	17.56	0.007	1.082	0.009
36	06:56:05.21	−13:16:29.75	16.74	0.002	16.20	0.002	15.52	0.003	1.084	−0.031
37	06:56:05.51	−13:13:29.11	19.69	0.009	18.49	0.005	17.11	0.004	1.089	−0.050
38	06:56:05.53	−13:15:09.85	19.45	0.008	18.60	0.005	17.47	0.007	0.921	−0.025
39	06:56:05.57	−13:15:18.62	18.47	0.004	17.62	0.003	16.52	0.005	1.142	−0.035
40	06:56:05.65	−13:15:11.24	19.32	0.007	18.46	0.004	17.33	0.006	1.103	−0.004
41	06:56:05.66	−13:14:26.70	18.30	0.003	16.89	0.003	15.26	0.004	1.273	−0.074
42	06:56:05.80	−13:16:23.78	18.84	0.004	18.02	0.003	16.94	0.005	1.095	0.046
43	06:56:05.85	−13:16:30.40	19.67	0.023	18.75	0.005	17.54	0.007	1.769	0.413
44	06:56:05.91	−13:15:08.33	19.10	0.015	18.21	0.004	17.05	0.005	1.701	0.493
45	06:56:05.91	−13:14:55.77	19.52	0.033	18.63	0.020	17.48	0.007	2.310	−0.213
46	06:56:06.16	−13:14:29.79	19.81	0.008	18.91	0.006	17.75	0.007	1.073	−0.042
47	06:56:06.17	−13:14:06.92	19.54	0.007	18.40	0.004	17.05	0.005	1.087	−0.039
48	06:56:06.32	−13:14:58.41	18.88	0.007	18.05	0.006	16.97	0.006	1.180	0.153
49	06:56:06.37	−13:15:24.27	17.25	0.002	15.86	0.003	14.24	0.004	1.603	−0.126
50	06:56:06.41	−13:15:51.58	16.56	0.002	15.14	0.002	13.52	0.045	6.578	0.075
51	06:56:06.51	−13:14:43.98	18.95	0.005	18.03	0.005	16.83	0.006	1.353	0.080
52	06:56:06.61	−13:13:15.27	20.35	0.015	18.88	0.007	17.20	0.006	1.025	0.008
53	06:56:06.62	−13:13:12.91	18.71	0.005	17.82	0.003	16.65	0.005	1.157	−0.038
54	06:56:06.63	−13:13:31.33	17.93	0.003	16.92	0.003	15.63	0.004	1.279	−0.105
55	06:56:06.67	−13:14:53.42	19.84	0.010	18.56	0.005	17.13	0.006	1.227	−0.083
56	06:56:06.95	−13:15:13.87	19.15	0.005	18.28	0.004	17.08	0.007	1.035	0.009
57	06:56:07.03	−13:16:04.54	19.68	0.008	18.82	0.005	17.67	0.007	1.083	−0.030
58	06:56:07.12	−13:15:48.73	18.75	0.006	17.88	0.003	16.74	0.004	1.192	0.111
59	06:56:07.21	−13:14:52.38	18.99	0.008	18.08	0.004	17.03	0.005	0.918	0.090

Table 2
Continued

ID	R.A. (J2000) hh:mm:ss	Dec. (J2000) dd:mm:ss	B	$\sigma(B)$	V	$\sigma(V)$	I	$\sigma(I)$	χ	sharpness
60	06:56:07.28	−13:14:53.50	19.53	0.010	18.57	0.005	17.32	0.006	0.909	0.052
61	06:56:07.46	−13:14:32.94	19.60	0.014	18.41	0.004	16.97	0.005	1.430	0.009
62	06:56:07.53	−13:13:12.23	18.18	0.003	17.29	0.003	16.12	0.004	1.126	−0.071
63	06:56:07.57	−13:13:40.53	19.14	0.005	18.32	0.004	17.17	0.006	1.155	−0.025
64	06:56:07.58	−13:14:39.80	18.88	0.005	18.03	0.004	16.90	0.005	1.103	0.021
65	06:56:07.63	−13:14:23.84	19.31	0.006	18.46	0.004	17.32	0.005	1.028	−0.076
66	06:56:07.93	−13:13:37.70	19.65	0.007	18.76	0.005	17.60	0.006	1.025	−0.065
67	06:56:08.14	−13:16:27.92	19.95	0.010	18.60	0.005	16.97	0.005	1.029	−0.058
68	06:56:08.23	−13:14:37.70	19.91	0.010	18.75	0.005	17.39	0.006	1.089	0.004
69	06:56:08.44	−13:16:27.10	18.09	0.003	17.21	0.003	16.03	0.004	1.099	−0.030
70	06:56:08.65	−13:14:44.54	18.85	0.005	17.97	0.003	16.84	0.004	1.001	−0.021
71	06:56:09.07	−13:14:46.01	17.22	0.002	16.37	0.003	15.30	0.003	1.372	−0.033
72	06:56:09.56	−13:13:57.52	19.16	0.005	18.51	0.005	17.65	0.008	1.169	−0.114
73	06:56:09.62	−13:15:22.41	19.26	0.047	18.36	0.021	17.19	0.012	4.276	2.010
74	06:56:09.64	−13:16:32.90	17.36	0.002	16.07	0.002	14.55	0.003	1.227	−0.073
75	06:56:09.71	−13:15:42.04	19.68	0.008	18.81	0.005	17.68	0.006	1.058	0.098
76	06:56:09.72	−13:14:09.50	19.82	0.008	18.76	0.005	17.44	0.006	1.042	0.066
77	06:56:10.02	−13:13:49.08	18.05	0.003	17.10	0.003	15.93	0.003	1.137	−0.077
78	06:56:10.05	−13:13:42.90	19.45	0.006	18.58	0.004	17.45	0.005	1.004	−0.012
79	06:56:10.24	−13:15:41.29	19.31	0.007	18.43	0.004	17.31	0.007	1.135	−0.014
80	06:56:10.24	−13:14:28.93	19.42	0.008	18.55	0.006	17.38	0.007	1.100	0.082
81	06:56:10.50	−13:13:56.56	20.10	0.010	18.63	0.005	16.88	0.004	1.047	−0.175
82	06:56:10.76	−13:15:55.35	20.06	0.010	18.73	0.005	17.26	0.006	1.127	−0.034
83	06:56:11.08	−13:15:46.69	19.38	0.006	18.52	0.004	17.45	0.005	0.985	0.024
84	06:56:11.30	−13:14:25.49	17.47	0.003	16.08	0.002	14.44	0.003	1.214	−0.058
85	06:56:11.40	−13:13:52.18	17.95	0.003	17.08	0.002	15.96	0.004	1.198	0.011
86	06:56:11.41	−13:15:40.76	19.71	0.007	18.82	0.005	17.68	0.008	1.092	−0.053
87	06:56:11.44	−13:14:24.73	19.82	0.012	18.90	0.009	17.66	0.012	0.598	−0.023
88	06:56:11.96	−13:14:12.16	17.24	0.002	16.35	0.002	15.20	0.003	1.199	−0.021
89	06:56:12.02	−13:13:41.90	19.22	0.006	18.36	0.004	17.21	0.005	1.047	−0.025
90	06:56:12.16	−13:14:52.31	16.12	0.002	15.40	0.002	14.54	0.003	1.330	−0.083
91	06:56:12.16	−13:14:14.52	19.92	0.010	18.80	0.005	17.44	0.006	0.954	−0.010
92	06:56:12.26	−13:15:10.06	18.89	0.005	17.72	0.003	16.38	0.004	1.174	−0.086

3.2. Color-Magnitude Diagrams

Figure 5 shows the $V-(B-V)$ (panel a), $V-(V-I)$ (panel b), $B-(B-V)$ (panel c), and $I-(V-I)$ (panel d) color-magnitude diagrams (CMDs) of the OC Ruprecht 6 for the radial range of $< 2'$ obtained in this study, while Figure 6 shows the comparison region ($3' < R < 3.6'$) with the same area. Some characteristic features that can be found for Ruprecht 6 in these CMDs are : (i) main-sequence (MS) stars are clearly seen and red dotted lines show the blue turn-off point at $B \approx 19.30$ mag, $V \approx 18.45$ mag, $I \approx 17.30$ mag, $B-V \approx 0.85$ mag, and $V-I \approx 1.15$ mag (see Figure 2 of Kaluzny (1994) for the definition of the blue turn-off), (ii) some red giant stars evolved after the turn-off are found, and (iii) three RC stars are seen and denoted as boxes in Figure 5 with mean magnitudes and colors of $B = 17.36 \pm 0.09$ mag, $V = 16.00 \pm 0.10$ mag, $I = 14.41 \pm 0.13$ mag, $B-V = 1.35 \pm 0.05$, mag $V-I = 1.59 \pm 0.05$ mag.

To further check the membership probability of the three RC stars statistically, we extracted all stars with similar magnitudes and colors to the RC stars in the whole observed area of $19.57' \times 19.57'$. Figure 7 shows the spatial distribution of the resultant 10 stars located in the RC box area of Figure 5 and Figure 6, including the three RC stars in Ruprecht 6. The stellar spatial density of the three stars in the cluster area is $3/(\pi \cdot 2^2) = 0.239$ arcmin^{-2}, while that of the seven stars outside of the cluster area is $7/(19.57^2 - \pi \cdot 2^2) = 0.019$ arcmin^{-2}. The stellar density of the cluster area is $0.239/0.019 = 12.58$ times higher than that of the background area, and thus we conclude that the three RC stars in Ruprecht 6 are members of the cluster with high probability.

3.3. Distance Estimation

Red clump giant stars are low-mass stars at the evolutionary stage of core-helium-burning. They define a sharp feature (almost constant absolute magnitude) in the CMDs of stellar systems like nearby galaxies and star clusters (Paczyński & Stanek 1998; Kim & Sung 2003; Kim et al. 2005; Kyeong et al. 2011; Karaali et al. 2013; Girardi 2016; Davies et al. 2017; but, see also Wan et al. 2015). In the near-infrared (NIR), especially in the K_S-band, the RC is known to have small dependence on metallicity and age, showing $M_{K_S} = -1.595 \pm 0.025$

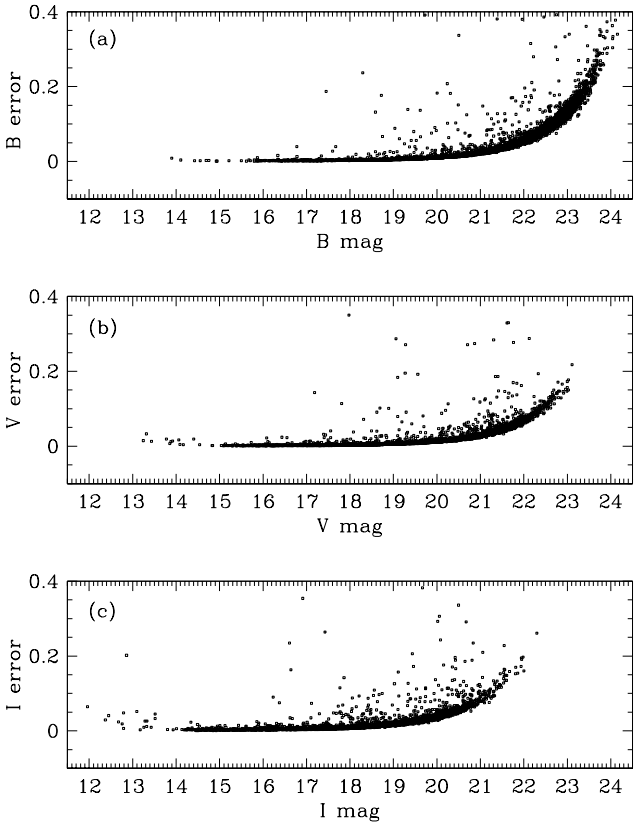

Figure 2. Error distributions of the B, V, and I-band photometry results as a function of magnitude. Only stars matched in all the three B, V, and I-bands are plotted.

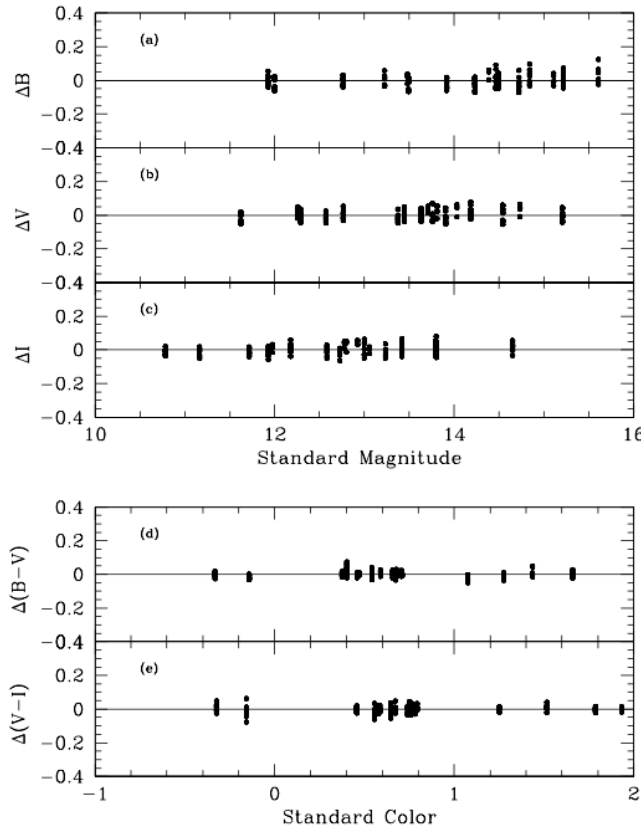

Figure 3. BVI residuals between standard and transformed magnitudes of the standard stars, plotted against standard magnitudes. Δ means standard magnitude (color) minus transformed magnitude (color).

mag and an intrinsic color of $(J-K_S)_0 = 0.612 \pm 0.003$ mag (Yaz Gökçe et al. 2013; Özdönmez et al. 2016). Recently, Girardi (2016) published a detailed review paper on the RC stars, and summarized the mean absolute magnitudes of these stars, which could possibly be used to estimate the distances and extinctions to stellar systems with the age of 1 to 10 Gyr though with some caveats such as population effects. Table 3 shows the mean I-band absolute magnitudes of RC stars from Girardi (2016) and the mean values of the five sources is $\langle M_I \rangle = -0.236 \pm 0.024$ mag.

Since it is known that the near-infrared K-band magnitude of the RC stars is not as sensitive to the age and metallicity of the star cluster as the optical I-band magnitude (Sarajedini 1999; Grocholski & Sarajedini 2002; Kyeong et al. 2011), we mainly used the mean K(RC) magnitude of the RC stars in Ruprecht 6. Table 4 shows the JHK_s magnitudes of the three RC stars in Ruprecht 6 extracted from the 2MASS (Two Micron All Sky Survey,[4] Skrutskie et al. 1997, 2006) data archive. Using the mean K(RC) magnitude of $\langle K_s \rangle = 12.39 \pm 0.21$, the extinction value of $A_V = 1.30$ (see Section 3.4), and the extinction ratio of $A_K = 0.118 A_V = 0.15$ (Dutra et al. 2002), we obtain a distance modulus of $(m-M)_0 = K_s - M_{K_s} - A_K = 12.39 - (-1.595) - 0.15 = 13.84 \pm 0.21$ ($d = 5.86 \pm 0.60$).

[4]See http://www.ipac.caltech.edu/2mass/releases/allsky

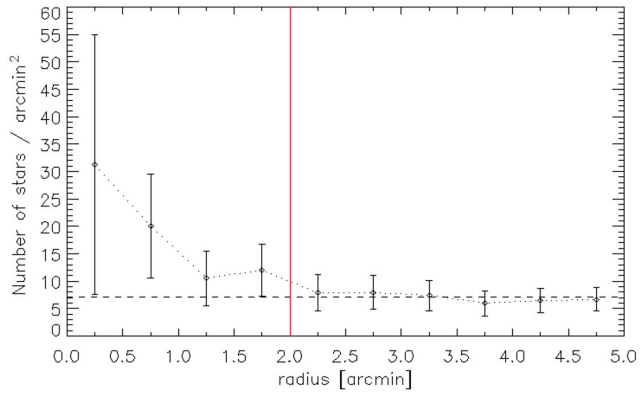

Figure 4. Radial number density profile for the stars with $V \leq 20$ mag in the field of the OC Ruprecht 6 with bin size of $0.5'$. The vertical red solid line represents our adopted size (radius) of the cluster ($2'$). Error bars denote the Poisson errors and the horizontal dashed line the level of field stellar density.

3.4. Reddening Estimation

For the estimation of the interstellar reddening value toward the OC Ruprecht 6, we adopted the following four methods. First, we have used the mean NIR color of the RC stars ($\langle J-K_s \rangle = 0.81 \pm 0.06$) from Table 4 and the intrinsic color of RC stars ($(J-K_s)_0 = 0.612 \pm 0.003$

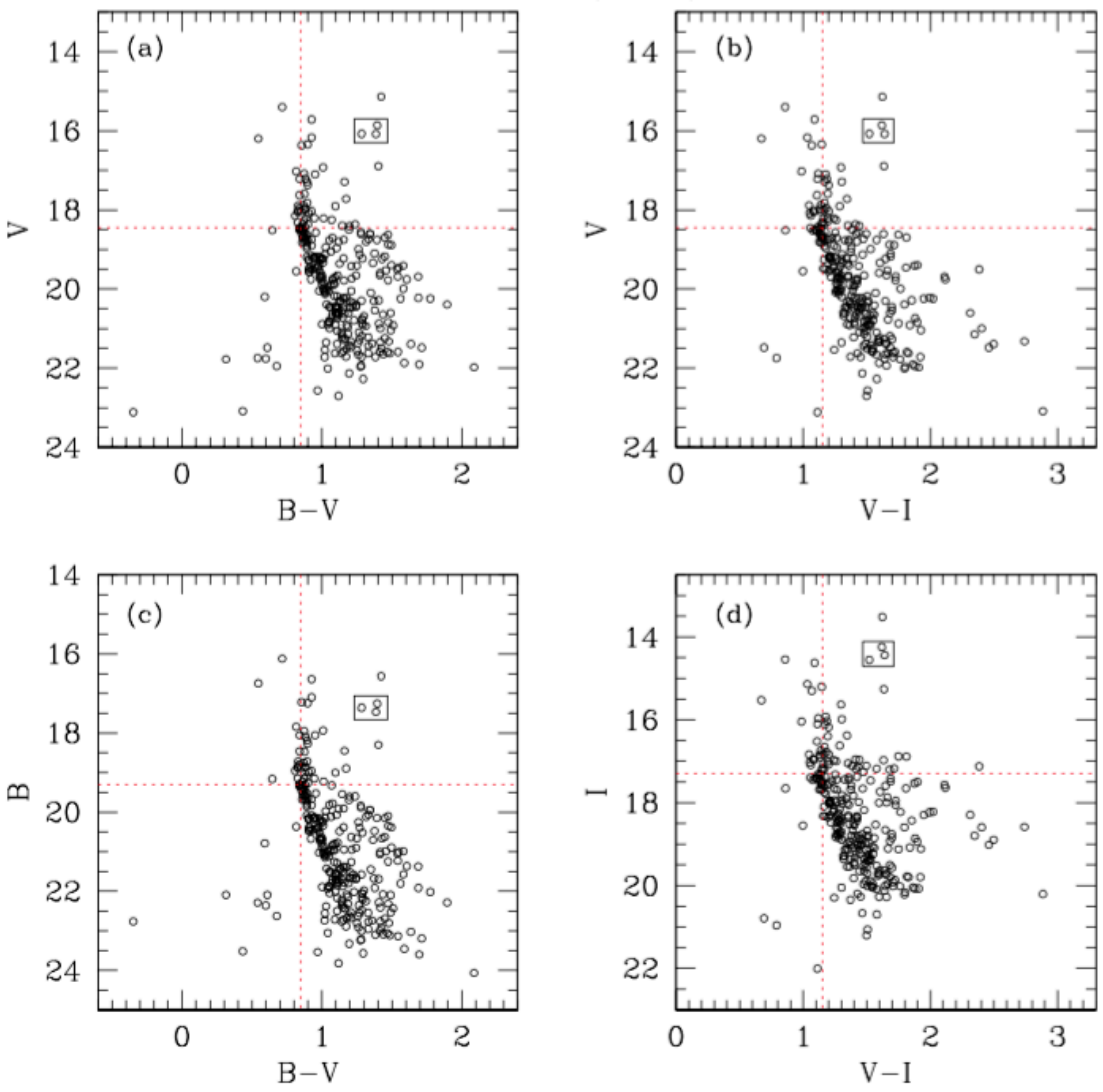

Figure 5. (a) $V-(B-V)$, (b) $V-(V-I)$, (c) $B-(B-V)$, and (d) $I-(V-I)$ color-magnitude diagrams for the 296 stars of the OC Ruprecht 6 within a radius $< 2'$. Red dotted lines show the main-sequence turn-off point at $B \approx 19.30$, $V \approx 18.45$, and $I \approx 17.30$ mag. Boxes show the location of the three red clump (RC) stars.

Table 3
Mean I-band absolute magnitudes of RC stars[†]

M_I	Reference	Comments
-0.279 ± 0.088	Paczyński & Stanek (1998)	Includes reddening correction
-0.23 ± 0.03	Stanek & Garnavich (1998)	Volume limited to 70 pc
-0.209	Girardi et al. (1998)	Lutz-Kelker bias corrected
-0.22 ± 0.03	Groenewegen (2008)	First uses revised *Hipparcos* parallaxes
-0.24 ± 0.01	Francis & Anderson (2014)	Peak of luminosity distribution

[†]From Girardi (2016). Values generally from *Hipparcos*.

mag) mentioned in Section 3.3, we obtain $E(J-K_s) = (J-K_s)-(J-K_s)_0 = 0.20 \pm 0.06$. Using the relation $E(J-K_s) = 0.488E(B-V)$ (Kim 2006), we obtain $E(B-V) = 0.41 \pm 0.06$.

Secondly, we have used the mean optical color of the RC stars in Ruprecht 6: $B-V = 1.35 \pm 0.05$ (Section 3.2). Janes & Phelps (1994) gave the mean color and magnitude of the RC stars in old OCs as $(B-V)_{0,RC} = 0.95 \pm 0.10$ and $M_{V,RC} = 0.90 \pm 0.40$, when the V magnitude difference between the RC stars and the MS turn-off of the clusters, δV, is greater than one (Kim & Sung 2003). Since $\delta V \approx 18.45 - 16.00 > 1$ for Ruprecht 6, we obtain $E(B-V) = (B-V)-(B-V)_0 = 1.35 - 0.95 = 0.40 \pm 0.11$.

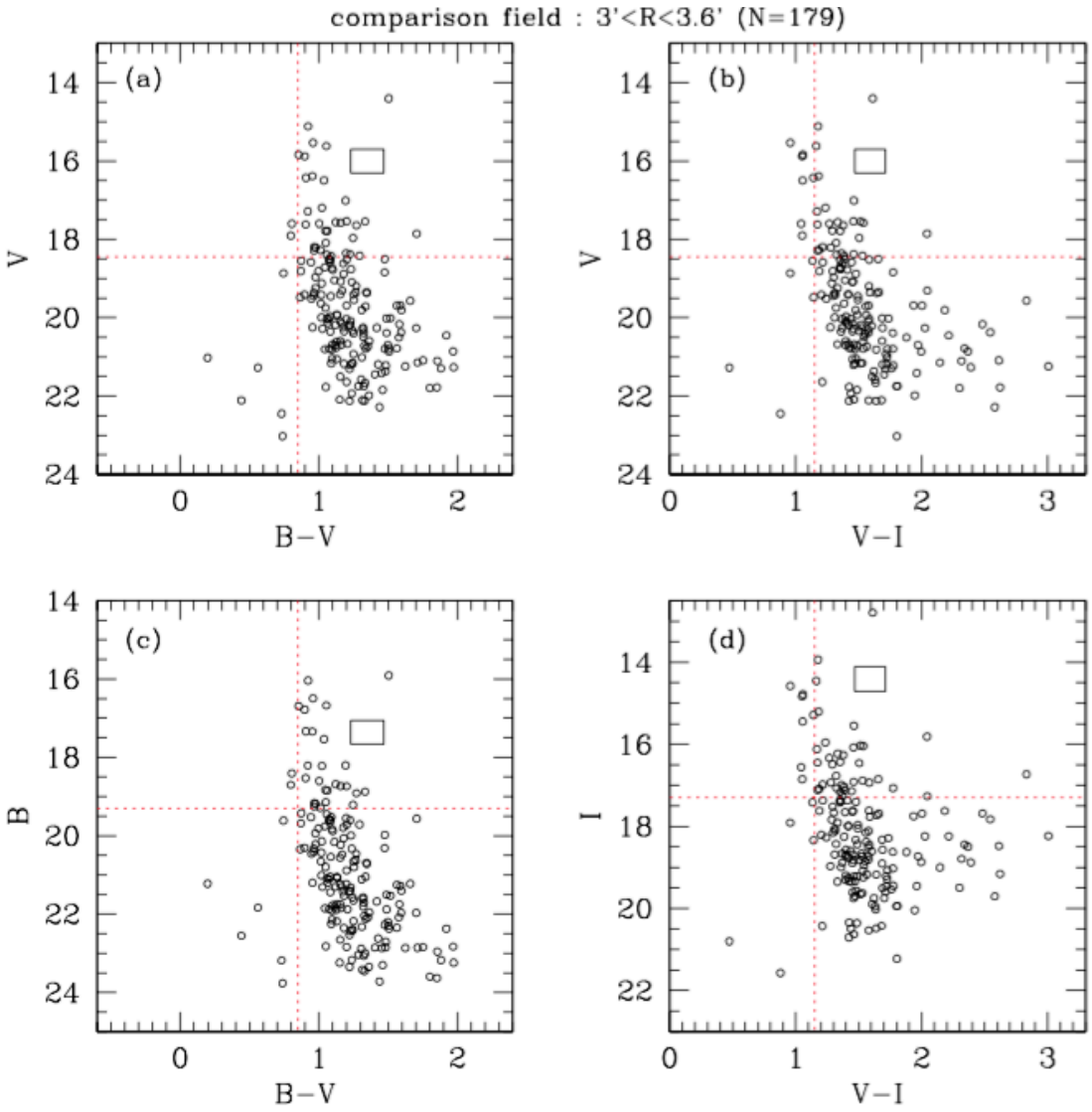

Figure 6. Same as in Figure 5, but for the comparison field of $3' <$ radius $< 3.6'$ around Ruprecht 6. This radius range gives the same area as in the case of Ruprecht 6. The red dotted lines and black boxes are the turn-off point and the region of the RC stars for Ruprecht 6 shown here just as a guide.

Table 4
2MASS Photometry of the RC stars in Ruprecht 6

IDs†	R.A.(J2000) hh:mm:ss	Decl.(J2000) dd:mm:ss	J	$\sigma(J)$	H	$\sigma(H)$	K_s	$\sigma(K_s)$	$J-K_s$
49	06:56:06.37	−13:15:24.27	13.004	0.023	12.350	0.026	12.120	0.024	0.884
74	06:56:09.64	−13:16:32.90	13.383	0.024	12.764	0.029	12.634	0.028	0.784
84	06:56:11.30	−13:14:25.49	13.184	0.026	12.564	0.027	12.400	0.029	0.749

†IDs from Table 2.

Thirdly, we have used the $(B-V)$ versus $(V-I)$ diagram of bright stars with $V < 19$ mag and stars of $19 < V < 20$ mag in Ruprecht 6 at radius $< 2'$ as shown in Figure 8. Solid and dotted lines show the intrinsic relations for the dwarf and giant stars, respectively, from Sung et al. (2013), which are shifted according to the reddenings of $E(B-V) = 0.40$ and $E(V-I) = 0.59$. Although the reddening vector in the diagram is very similar to the distribution of MS and giant stars, we can get a hint of the amount of the reddening values from this diagram. From the comparison of the observed colors of the bright stars of Ruprecht 6 and the intrinsic colors, we derive the reddening values of $E(B-V) = 0.40 \pm 0.10$ and $E(V-I) = 0.59 \pm 0.10$.

Finally, PARSEC isochrone fittings are made as shown in Section 3.5, which gives the best match with

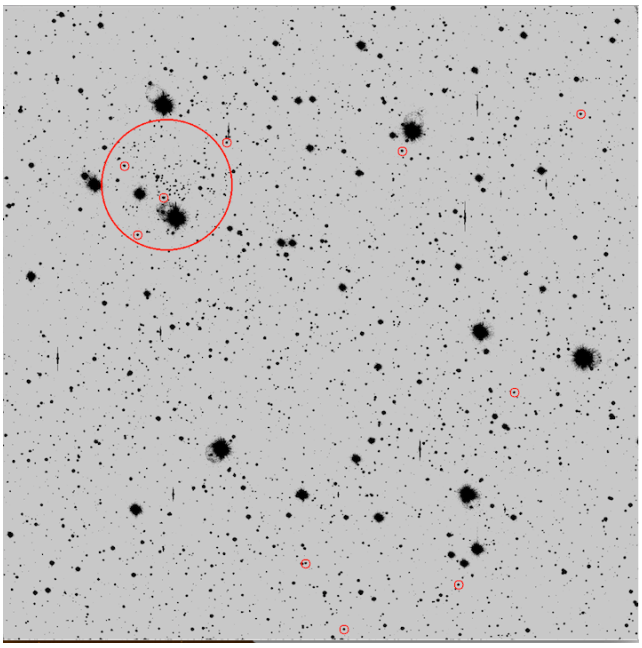

Figure 7. V-band grey-scale images of the open cluster Ruprecht 6 with the same thick and large red circle as in Figure 1 (radius of 2′). Small red circles show the 10 stars with magnitudes and colors located in the boxed area of the RC stars in the CMDs of Figure 5 and Figure 6. Note that three stars, out of 10, are located in the small area of the radial content of Ruprecht 6.

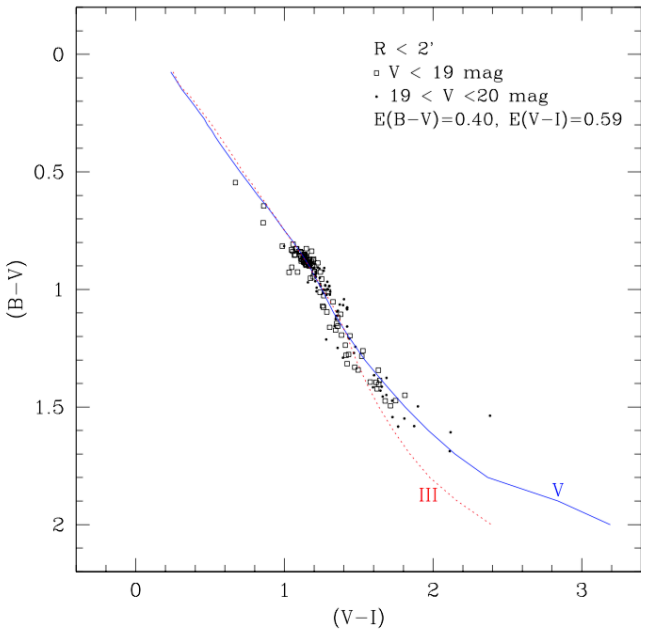

Figure 8. $(B-V)$ versus $(V-I)$ diagram for the bright ($V < 19$ mag, open squares) and less bright ($19 < V < 20$ mag, dots) stars of the OC Ruprecht 6 at radius $< 2'$. Solid and dotted lines represent the intrinsic relations for the dwarf and giant stars, respectively, from Sung et al. (2013), which are shifted according to the reddenings of $E(B-V) = 0.40$ and $E(V-I) = 0.59$.

$E(B-V) = 0.42$ and $E(V-I) = 0.60$, which are in agreement with the values above within uncertainties.

Considering the results of these four methods, we assume that the true reddening values toward Ruprecht 6 are in the range of $E(B-V) = 0.40-0.42$ and $E(V-I) = 0.59-0.60$, and in this study we adopt the values of $E(B-V) = 0.42$ and $E(V-I) = 0.60$ which afford the best isochrone matches (see Section 3.5). This is in very good agreement with the value ($E(B-V) = 0.43$) listed in the DAML02 catalog. The interstellar extinction laws given by Cardelli et al. (1989) are used to calculate the extinctions for other colors for the total-to-selective extinction ratio of $R_V = 3.1$: $A_B = 4.14E(B-V) = 1.74$, $A_V = 3.10E(B-V) = 1.30$, $A_I = 1.48E(B-V) = 0.62$ (Lee & Kim 2000; Kim et al. 2012).

3.5. PARSEC Isochrone Fittings

In Figure 9, we have plotted the V versus $(B-V)$ (a), V versus $(V-I)$ (b), B versus $(B-V)$ (c), and I versus $(V-I)$ (d) CMDs for Ruprecht 6 together with the theoretical PAdova and TRieste Stellar Evolution Code (PARSEC) isochrones (Bertelli et al. 1994; Girardi et al. 2000, 2002; Bressan et al. 2012). The best matched isochrones are for the parameters of [Fe/H] $= -0.42 \pm 0.04$ dex and log (age) $= 9.50 \pm 0.10$ (t $= 3.16 \pm 0.82$ Gyr) shifted using $E(B-V) = 0.42$, $E(V-I) = 0.60$, $B-M_B = 15.58$, $V-M_V = 15.14$, and $I-M_I = 14.46$. The metallicity and age values obtained in this study are in excellent agreement with those of Hasegawa et al. (2008) ([Fe/H] $= -0.41$ and log (t) $= 9.50$, t $= 3.2$ Gyr) and DAML02 ([Fe/H] $= -0.38$ and log (t) $= 9.50$).

With the limited data of BVI photometry only, it is not an easy task to determine the reddening, distance, age, and metallicity simultaneously from the isochrone fitting due to the degeneracy of parameters. We, therefore, have used pre-determined values of distance (Section 3.3) and reddening (Section 3.4) for the isochrone fittings just to find optimum values of age and metallicity, after which slight fine-tunings are made. Good matches of the theoretical isochrones and the observed photometry data lend support for the distance and reddening values, and the newly obtained values of age and metallicity.

4. Discussion

4.1. Red Clump Stars

Among the 10 RC stars shown in Figure 7, one star is located just outside of the 2′ radius circle of Ruprecht 6, with its coordinates R.A. $(J2000) = 06^h\ 56^m\ 6.366^s$ and Decl. $(J2000) = -13°\ 15'\ 24.27''$. Since it is very likely that this star could also be a member of the cluster considering its close location to the cluster area, we can include it in our estimation of the cluster parameters. The optical and 2MASS NIR photometry results of the star are : $B = 17.358 \pm 0.003$ mag, $V = 15.912 \pm 0.002$ mag, $I = 14.273 \pm 0.004$ mag, $J = 12.981 \pm 0.026$ mag, $H = 12.229 \pm 0.022$ mag, $K_S = 12.065 \pm 0.024$ mag, and $(J-K_s) = 0.916$ mag.

Inclusion of this star gives a mean $K_s(RC)$ magnitude of $\langle K_s \rangle = 12.31 \pm 0.23$ mag. This gives the

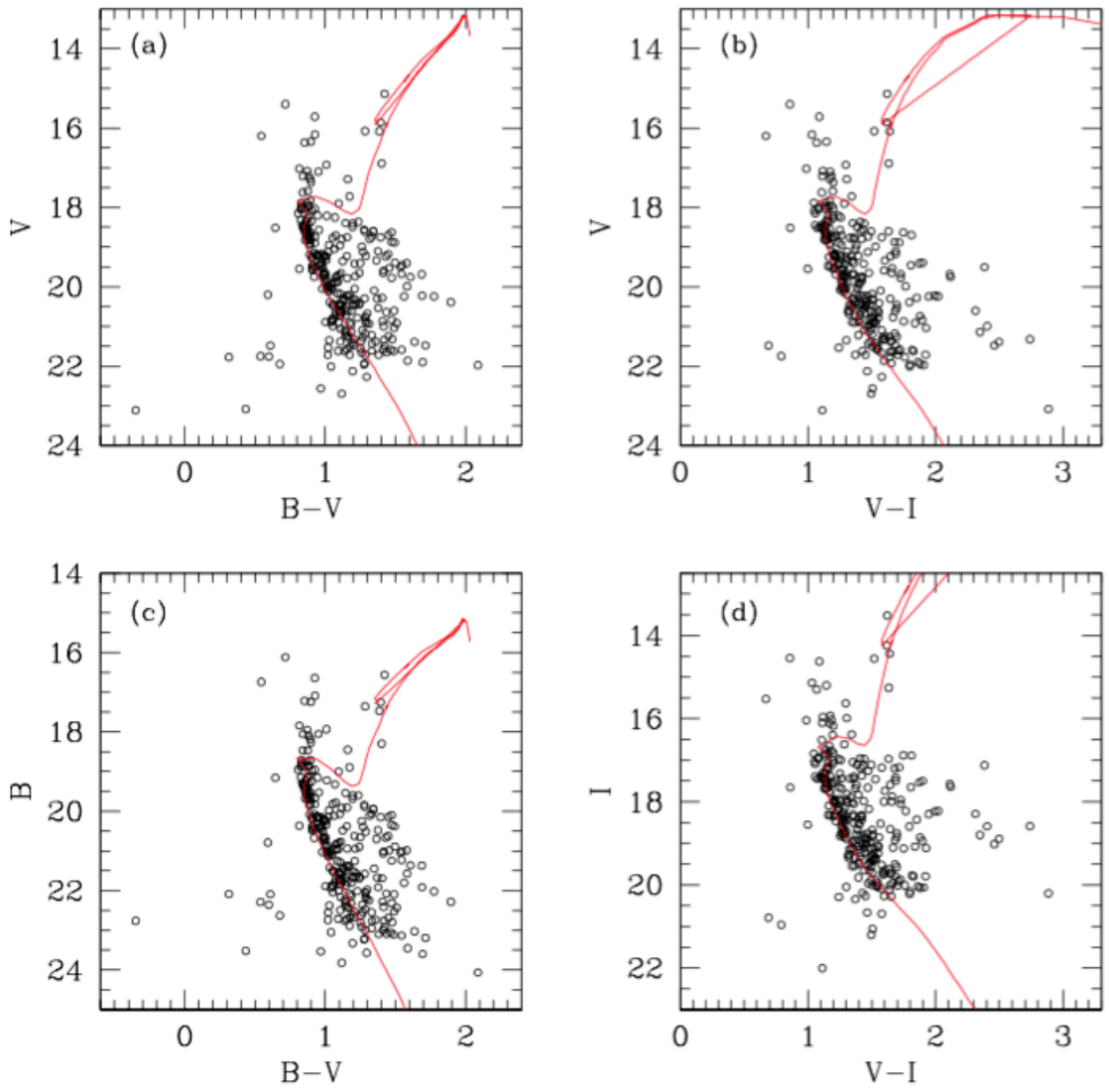

Figure 9. PARSEC isochrone fittings onto the color-magnitude diagrams of Ruprecht 6 for (a) $V-(B-V)$, (b) $V-(V-I)$, (c) $B-(B-V)$, and (d) $I-(V-I)$ parameter space. Open circles are the 296 stars of Ruprecht 6 at radius $< 2'$. The red solid lines show the PARSEC isochrones of log (age) = 9.50 (t = 3.16 Gyr) and [Fe/H] = −0.42 dex shifted according to $E(B-V) = 0.42$, $E(V-I) = 0.60$, $B - M_B = 15.58$, $V - M_V = 15.14$, and $I - M_I = 14.46$.

distance modulus of $(m-M)_0 = K_s - M_{K_s} - A_K = 12.31 - (-1.595) - 0.15 = 13.76 \pm 0.23$ ($d = 5.65 \pm 0.63$ kpc, still using the reddening values obtained in Section 3.4), which agrees within the error range but is somewhat shorter than that in Section 3.3. The mean NIR color of the four RC stars including the above one is $\langle(J-K_s)\rangle = 0.83 \pm 0.07$ mag and this results in slightly larger reddening values of $E(J-K_s) = (J-K_s) - (J-K_s)_0 = 0.22 \pm 0.07$ and $E(B-V) = 0.45 \pm 0.07$.

4.2. Galactocentric Metallicity Distribution

OCs have been used as one of the tools to probe the Galactocentric radial metallicity distribution in our own Galaxy (Kim & Sung 2003; Wu et al. 2009; Ryu & Lee 2011). This radial variation of the metallicity in the disk of the Galaxy is a powerful tool for the understanding of the star formation and chemical evolution of the system (Fernández-Martín et al. 2017). Kim et al. (2005) have compiled the slope ($= \Delta$[Fe/H]$/\Delta R_{\rm GC}$) values of the Galactocentric radial metallicity gradient published up to then. Using the nine published slope values, they obtained the mean value of the slope Δ[Fe/H]$/\Delta R_{\rm GC} = -0.066 \pm 0.019$. In Table 5, we have compiled again the slopes and intercept values incorporating recently published results for OCs.

For the OCs in the DAML02 catalog, we have calculated the Galactocentric distances using the distance estimates, Galactic coordinates in the catalog, and the equation

$$R_{\rm GC}^2 = [d\cos(b)\cos(l) - R_0]^2 + d^2\cos^2(b)\sin^2(l) + d^2\sin^2(b)$$

where d is the heliocentric distance to the cluster, l and b are the Galactic longitude and Galactic latitude, respectively, of the cluster, R_0 is the distance of the

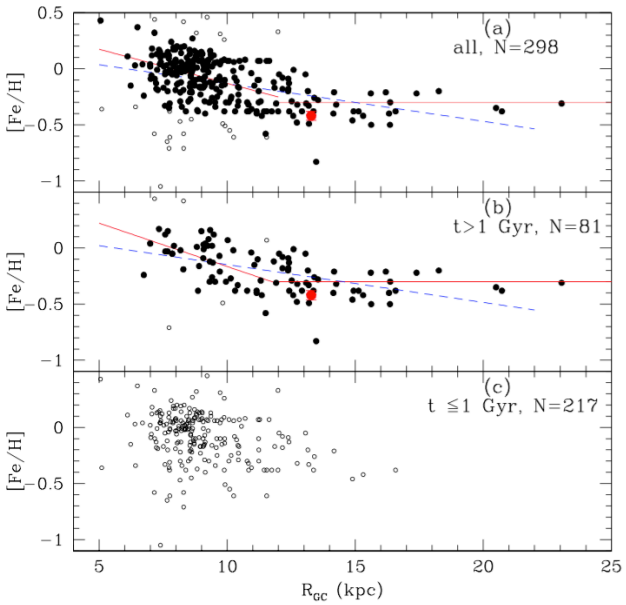

Figure 10. Galactocentric radial distribution of the OCs in the Milky Way. Data come from the DAML02 catalog for OCs with both Galactocentric radius ($R_{\rm GC}$) and metallicity ([Fe/H]) values. Panel (a) is for all the 298 OCs, panel (b) is only for the 81 old (age > 1 Gyr) OCs, and panel (c) is for the young (age ≤ 1 Gyr) OCs. Blue dashed lines are the least square fittings for all the data for the whole radial range. Panels (a) and (b) show that OCs in the outer region of $R > 12$ kpc might show almost constant metallicity value ([Fe/H] ~ -0.3 dex) regardless of the radius, while the red solid lines for the inner region of $R < 12$ kpc are the least square fittings only for the OCs that remained after 2σ clipping (N=231 for panel (a) and N=49 for panel (b)). Small open circles at $R < 12$ kpc in (a) and (b) denote the OCs excluded during the 2σ clipping process. The large red dot with error bars immersed inside represents the position of Ruprecht 6 with parameters obtained in this study.

Sun from the Galactic center (8.5 kpc is used in this study). Out of 2167 OCs listed in the DAML02 catalog, only 298 clusters have both of metallicity and distance estimates, which are shown in Figure 10 as a function of the Galactocentric distance, $R_{\rm GC}$.

We have performed the least square fitting for all 298 OCs with both metallicity and distance estimates, and obtained [Fe/H] $= (-0.034 \pm 0.005) R_{\rm GC} + (0.204 \pm 0.053)$ with rms = 0.229 for the entire radial range of the Galaxy (shown as blue dashed line in Figure 10 (a)). Assuming the outer ($R > 12$ kpc) clusters might follow a constant ([Fe/H] ~ -0.3 dex) metallicity trend, we also made the least square fitting only for the inner ($R_{\rm GC} < 12$ kpc) OCs with 2σ clipping, which returns [Fe/H] $= (-0.061 \pm 0.008) R_{\rm GC} + (0.479 \pm 0.071)$ with rms = 0.155 (N = 231) (shown as red solid line in Figure 10 (a)).

Taking into account only the old OCs with age > 1 Gyr, we plotted the same thing in Figure 10 (b). The 81 objects in the whole radial range give the relation of [Fe/H] $= (-0.034 \pm 0.007) R_{\rm GC} + (0.190 \pm 0.080)$ with rms = 0.201 (blue dashed line in Figure 10 (b)), and the 49 clusters at $R_{\rm GC} < 12$ kpc left after the 2σ clipping process returns [Fe/H] $= (-0.077 \pm 0.017) R_{\rm GC} + (0.609 \pm 0.161)$ with rms = 0.152 (red solid line in Figure 10 (b)). This result is in very good agreement with those obtained recently by Ryu & Lee (2011) and Andreuzzi et al. (2011), while the number of OCs used in this study is smaller than those of the previous studies because of our process of extracting only the old and good (by 2σ clipping) clusters for the analysis.

Ruprecht 6 is shown as a large red dot with error bars immersed in Figure 10 (a) and (b). Whether we adopt the single relation for the whole radial range or the dual relation broken at $R_{\rm GC} \sim 12$ kpc, Ruprecht 6 seems to conform to either of the radial metallicity trends at its location of $R_{\rm GC} = 13.28 \pm 0.54$ kpc.

The metallicity estimates from photometric indices are less reliable than those from spectroscopic observations. $(U - B)$ colors for late-F to early-K-type stars, Washington and DDO photometric systems for G and K-type giants can give some reliable values. However, while the DAML02 catalog gives detailed references for proper motions and radial velocities, the sources for the metallicity estimates are not listed. Among the 81 objects in Figure 10 (b), there are 18 objects for which $N \geq 10$ stars are used to determine the metallicity, 40 objects for which $1 \leq N \leq 9$ stars are used, and no information is given for the other 23 objects. Investigating the sources of the metallicity estimates again is beyond the scope of this paper, but a compilation and classification of these estimates using the criteria of the methods to find abundances and number of stars used will be a good approach to obtain a more reliable Galactocentric radial metallicity distribution of the OCs in the Milky Way.

5. Summary

We derived the physical parameters of the small-size and poorly studied old OC Ruprecht 6 using the *BVI* optical photometry data. The main results obtained in this study are:

- The color-magnitude diagrams of Ruprecht 6 show clear MS stars. The MS turn-off point is at $V \approx 18.45$ mag and $B - V \approx 0.85$ mag.
- Three RC stars are at $V = 16.00$ mag, $I = 14.41$ mag and $B - V = 1.35$ mag. The mean K_s-band magnitude of RC stars ($K_s = 12.39 \pm 0.21$ mag) and the known absolute magnitude of the RC stars ($M_{K_S} = -1.595 \pm 0.025$ mag) gives the distance modulus of $(m - M)_0 = 13.84 \pm 0.21$ mag ($d = 5.86 \pm 0.60$ kpc) to Ruprecht 6.
- From the $(J - K_s)$ and $(B - V)$ colors of the RC stars, comparison of the $(B - V)$ and $(V - I)$ colors of the bright stars in Ruprecht 6 with those of the intrinsic colors of dwarf and giant stars, and the PARSEC isochrone fittings, we derive the reddening values of $E(B-V) = 0.42$ mag and $E(V-I) = 0.60$ mag.
- Using the PARSEC isochrone fittings onto the color-magnitude diagrams, we obtain the age and

Table 5
Slope and intercept values in the equation of $< [Fe/H] >= a \times R_{\rm GC} + b$

Reference	Radial Coverage	a	b	RMS	N
This study	All	-0.034 ± 0.007	0.190 ± 0.080	0.201	81
This study	$R < 12$ kpc	-0.077 ± 0.017	0.609 ± 0.161	0.152	49
This study	$R > 12$ kpc	0	-0.3	–	27
Ryu & Lee (2011)	$R < 12$ kpc	-0.076 ± 0.013	0.600 ± 0.116	0.029	186
Ryu & Lee (2011)	$R > 12$ kpc	0	-0.3		186
Andreuzzi et al. (2011)	All	-0.04	–	–	177
Andreuzzi et al. (2011)	$R < 12$ kpc	-0.07	–	–	177
Andreuzzi et al. (2011)	$R > 12$ kpc	0	-0.35	–	177
Kim (2006)	All	-0.067 ± 0.009	–	–	53
Kim et al. (2005)	All	-0.064 ± 0.009	–	–	51
Kim et al. (2005)	–	-0.066 ± 0.019	–	–	†
Friel et al. (2002)	All	-0.059 ± 0.010	–	–	39
Piatti et al. (1995)	All	-0.07 ± 0.01	–	0.13	63

The slope a ($= \Delta$[Fe/H]$/\Delta R_{\rm GC}$) is in units of dex kpc^{-1}.
† Mean value of the nine literature values.

metallicity values to be : log (t) = 9.50 ± 0.10 (t = 3.16 ± 0.82 Gyr) and [Fe/H] = -0.42 ± 0.04 dex.

- For the old (age > 1 Gyr) OCs of DAML02 catalog, we obtain the Galactocentric radial metallicity relations of either (i) a single relation of [Fe/H] = $(-0.034 \pm 0.007) R_{\rm GC} + (0.190 \pm 0.080)$ (rms = 0.201) or (ii) dual relation of [Fe/H] = $(-0.077 \pm 0.017) R_{\rm GC} + (0.609 \pm 0.161)$ (rms = 0.152) at $R_{\rm GC} < 12$ kpc and constant ([Fe/H] ~ -0.3 dex) value at $R_{\rm GC} > 12$ kpc.

ACKNOWLEDGMENTS

We thank the anonymous referee and the Scientific Editor for the thorough review and helpful comments that helped to improve the manuscript. The participation of I. H. and S. K. in this project was made possible by a UST Research Internship for Undergraduates grant in 2016 July. Based on observations at Cerro Tololo Inter-American Observatory, National Optical Astronomy Observatory (NOAO Prop. ID 2010B-0178, PI Sang Chul Kim), which is operated by the Association of Universities for Research in Astronomy (AURA) under a cooperative agreement with the National Science Foundation. This publication makes use of data products from the Two Micron All Sky Survey, which is a joint project of the University of Massachusetts and the Infrared Processing and Analysis Center/California Institute of Technology, funded by the National Aeronautics and Space Administration and the National Science Foundation.

REFERENCES

Anders, F., Chiappini, C., Minchev, I., et al. 2017, Red Giants Observed by CoRoT and APOGEE: The Evolution of the Milky Way's Radial Metallicity Gradient, A&A, 600, A70

Andreuzzi, G., Bragaglia, A., Tosi, M., et al. 2011, Old Open Clusters and the Galactic Metallicity Gradient: Berkeley 20, Berkeley 66 and Tombaugh 2, MNRAS, 412, 1265

Andrievsky, S. M., Luck, R. E., Martin, P., et al. 2004, The Galactic Abundance Gradient from Cepheids. V. Transition Zone between 10 and 11 kpc, A&A, 413, 159

Bertelli, G., Bressan, A., Chiosi, C., et al. 1994, Theoretical Isochrones from Models with New Radiative Opacities, A&AS 106, 275

Bressan, A., Marigo, P., Girardi, L., et al. 2012, PARSEC: Stellar Tracks and Isochrones with the PAdova and TRieste Stellar Evolution Code, MNRAS, 427, 127

Cantat-Gaudin, T., Donati, P., Vallenari, A., et al. 2016, Abundances and Kinematics for Ten Anticentre Open Clusters, A&A, 588, A120

Cardelli, J. A., Clayton, G. C., & Mathis, J. S. 1989, The Relationship between Infrared, Optical, and Ultraviolet Extinction, ApJ, 345, 245

Carraro, G., Geisler, D., Villanova, S., et al. 2007, Old Open Clusters in the Outer Galactic Disk, A&A, 476, 217

Cescutti, G., Matteucci, F., François, P., et al. 2007, Abundance Gradients in the Milky Way for α Elements, Iron Peak Elements, barium, lanthanum, and europium, A&A, 462, 943

Chen, L., Hou, J. L., & Wang, J. J. 2003, On the Galactic Disk Metallicity Distribution from Open Clusters. I. New Catalogs and Abundance Gradient, AJ, 125, 1397

Davies, G. R., Lund, M. N., Miglio, A., et al. 2017, Using Red Clump Stars to Correct the Gaia DR1 Parallaxes, A&A, 598, L4

Dias, W. S., Alessi, B. S., Moitinho, A., & Lepine, J. R. D. 2002, New Catalogue of Optically Visible Open Clusters and Candidates, A&A, 389, 871

Dutra, C. M., Santiago, B. X., & Bica, E. 2002, Low-Extinction Windows in the Inner Galactic Bulge, A&A, 381, 219

Fernández-Martín, A., Pérez-Montero, E., Vílchez, J. M., et al. 2017, 2017, Chemical Distribution of H II Regions towards the Galactic Anticentre, A&A, 597, A84

Francis, C., & Anderson, E. 2014, Two Estimates of the Distance to the Galactic Centre, MNRAS, 441, 1105

Friel, E. D., Janes, K. A., Tavarez, M., et al. 2002, Metallicities of Old Open Clusters, AJ, 124, 2693

Girardi, L. 2016, Red Clump Stars, ARA&A, 54, 95

Girardi, L., Groenewegen, M. A. T., Weiss, A., et al. 1998, Fine Structure of the Red Giant Clump from HIPPARCOS

Data, and Distance Determinations Based on Its Mean Magnitude, MNRAS, 301, 149

Girardi, L., Bressan, A., Bertelli, G., et al. 2000, Evolutionary Tracks and Isochrones for Low- and Intermediate-Mass Stars: From 0.15 to 7 $M_{\odot}$, and from Z=0.0004 to 0.03, A&AS, 141, 371

Girardi, L., Bertelli, G., Bressan, A., et al. 2002, Theoretical Isochrones in Several Photometric Systems. I. Johnson-Cousins-Glass, HST/WFPC2, HST/NICMOS, Washington, and ESO Imaging Survey Filter Sets, A&A, 391, 195

Grocholski, A. J., & Sarajedini, A. 2002, WIYN Open Cluster Study. X. The K-Band Magnitude of the Red Clump as a Distance Indicator, AJ, 123, 1603

Groenewegen, M. A. T. 2008, The Red Clump Absolute Magnitude Based on Revised Hipparcos Parallaxes, A&A, 488, 935

Hasegawa, T., Sakamoto, T., & Malasan, H. L. 2008, New Photometric Data of Old Open Clusters II. A Dataset for 36 Clusters, PASJ, 60, 1267

Janes, K. A., & Phelps, R. L. 1994, The Galactic System of Old Star Clusters: The Development of the Galactic Disk, AJ, 108, 1773

Jacobson, H. R., Friel, E. D., Jílková, L., et al. 2016, The Gaia-ESO Survey: Probes of the Inner Disk Abundance Gradient, A&A, 591, A37

Kaluzny, J. 1994, CCD Photometry of Distant Open Clusters. I. Berkeley 22, Berkeley 29 and Berkeley 54, A&AS, 108, 151

Karaali, S., Bilir, S., Yaz Gökçe, E. 2013, Absolute Magnitude Calibration for Red Clump Stars, Ap&SS, 346, 89

Kharchenko, N. V., Piskunov, A. E., Schilbach, E., et al. 2013, Global Survey of Star Clusters in the Milky Way. II. The Catalogue of Basic Parameters, A&A, 558, A53

Kim, S. C. 2006, Near-Infrared Photometric Study of the Galactic Open Clusters NGC 1641 and NGC 2394 Based on 2MASS Data, JKAS, 39, 115

Kim, S. C., & Sung, H. 2003, Physical Parameters of the Old Open Cluster Trumpler 5, JKAS, 36, 13

Kim, S. C., Park, H. S., Sohn, S. T., et al. 2005, BOAO Photometric Survey of Galactic Open Clusters. III. Czernik 24 and Czernik 27, JKAS, 38, 429

Kim, S. C., Kyeong, J., & Sung, E.-C. 2009, Near-Infrared Photometric Study of the Old Open Cluster Trumpler 5, JKAS, 42, 135

Kim, S. C., Park, H. S., Kyeong, J., et al. 2012, Distance and Reddening of the Isolated Dwarf Irregular Galaxy NGC 1156, PASJ, 64, 23

Krisciunas, K., Monteiro, H., & Dias, W. 2015, CCD Photometry of NGC 2482 and Five Previously Unobserved Open Star Clusters, PASP, 127, 31

Kyeong, J., Moon, H.-K., Kim, S. C., et al. 2011, 2MASS Near-IR Color-Magnitude Diagram of the Old Open Cluster King 11, JKAS, 44, 33

Landolt, A. U. 1992, $UBVRI$ Photometric Standard Stars in the Magnitude Range $11.5 - 16.0$ around the Celestial Equator, AJ, 104, 340

Landolt, A. U., & Uomoto, A. K. 2007, Optical Multicolor Photometry of Spectrophotometric Standard Stars, AJ, 133, 768

Landolt, A. U. 2009, UBVRI Photometric Standard Stars Around the Celestial Equator: Updates and Additions, AJ, 137, 4186

Lang, D., Hogg, D. W.; Mierle, K., Blanton, M., & Roweis, S. 2010, Astrometry.net: Blind Astrometric Calibration of Arbitrary Astronomical Images, AJ, 139, 1782

Lee, M. G., & Kim, S. C. 2000, Stellar Populations of the Sagittarius Dwarf Irregular Galaxy, AJ, 119, 777

Lyngå, G. 1987, Catalogue of Open Cluster Data (Observatoire de Strassbourg, Centre de Données Stellaires)

Netopil, M., Paunzen, E., Heiter, U., et al. 2016, On the Metallicity of Open Clusters. III. Homogenised Sample, A&A, 585, A150

Oliveira, A. F., Monteiro, H., Dias, W. S., et al. 2013, Fitting Isochrones to Open Cluster Photometric Data. III. Estimating Metallicities from UBV Photometry, A&A, 557, A14

Önal Taş, Ö., Bilir, S., Seabroke, G. M., et al. 2016, Local Stellar Kinematics from RAVE Data - VII. Metallicity Gradients from Red Clump Stars, PASA, 33, 44

Özdönmez, A., Güver, T., Cabrera-Lavers, A., et al. 2016, The Distances of the Galactic Novae, MNRAS, 461, 1177

Paczyński, B., & Stanek, K. Z. 1998, Galactocentric Distance with the Optical Gravitational Lensing Experiment and HIPPARCOS Red Clump Stars, ApJ, 494, L219

Park, H. S., & Lee, M. G. 1999, $UBVI$ Charge-Coupled Device Photometry of Two Old Open Clusters NGC 1798 and 2192, MNRAS, 304, 883

Paunzen, E., Heiter, U., Netopil, M., et al. 2010, On the Metallicity of Open Clusters I. Photometry, A&A, 517, A32

Piatti, A. E., Claria, J. J., Abadi, M. G. 1995, Chemical Evolution of the Galactic Disk: Evidence for a Gradient Perpendicular to the Galactic Plane, AJ, 110, 2813

Piskunov, A. E., Kharchenko, N. V., Röser, S., et al. 2006, Revisiting the Population of Galactic Open Clusters, A&A, 445, 545

Rudolph, A., Fich, M., Bell, G. R., et al. 2006, Abundance Gradients in the Galaxy, ApJS, 162, 346

Ruprecht, J. 1966 Classification of Open Star Clusters, Bull. Astron. Inst. Czech., 17, 33

Ryu, J., & Lee, M. G. 2011, A Photometric Study of Five Open Clusters in the SDSS, JKAS, 44, 177

Sarajedini, A. 1999, WIYN Open Cluster Study. III. The Observed Variation of the Red Clump Luminosity and Color with Metallicity and Age, AJ, 118, 2321

Skrutskie, M. F., Schneider, S. E., Stiening, R., et al. 1997, The Two Micron All Sky Survey (2MASS): Overview and Status, in The Impact of Large Scale Near-IR Sky Surveys, eds. F. Garzón, N. Epchtein, A. Omont, B. Burton and P. Persi, Kluwer (Dordrecht: Kluwer Academic Publishing Company), 25

Skrutskie, M. F., Cutri, R. M., Stiening, R., et al. 2006, The Two Micron All Sky Survey (2MASS), AJ, 131, 1163

Stanek, K. Z., & Garnavich, P. M. 1998, Distance to M31 with the Hubble Space Telescope and HIPPARCOS Red Clump Stars, ApJ, 503, L131

Stanghellini, L., & Haywood, M. 2010, The Galactic Structure and Chemical Evolution Traced by the Population of Planetary Nebulae, ApJ, 714, 1096

Stetson, P. B. 1990, On the Growth-Curve Method for Calibrating Stellar Photometry with CCDs, PASP, 102, 932

Sung, H., Lim, B., Bessell, M. S., et al. 2013, Sejong Open Cluster Survey (SOS). 0. Target Selection and Data Analysis, JKAS, 46, 103

Tadross, A. L. 2003, Metallicity Distribution on the Galactic Disk, NewA, 8, 737

Tadross, A. L. 2011, A Catalog of 120 NGC Open Star Clusters, JKAS, 44, 1

Tissera, P. B., Machado, R. E. G., Sanchez-Blazquez, P., et al. 2016, The Stellar Metallicity Gradients in Galaxy Discs in a Cosmological Scenario, A&A, 592, A93

Trumpler, R. J. 1930, Preliminary Results on the Distances, Dimensions and Space Distribution of Open Star Clusters, LicOB, 14, 154

Twarog, B. A., Ashman, K. M., Anthony-Twarog, B. J. 1997, Some Revised Observational Constraints on the Formation and Evolution of the Galactic Disk, AJ, 114, 2556

Wan, J.-C., Liu, C., Deng, L.-C., et al. 2015, Red Clump Stars from the LAMOST Data I: Identification and Distance, RAA, 15, 1166

Wu, Z.-Y., Zhou, X., Ma, J., et al. 2009, The Orbits of Open Clusters in the Galaxy, MNRAS, 399, 2146

Xiang, M.-S., Liu, X.-W., Yuan, H.-B., et al. 2015, The Evolution of Stellar Metallicity Gradients of the Milky Way Disk from LSS-GAC Main Sequence Turn-Off Stars: a Two-Phase Disk Formation History?, RAA, 15, 1209

Yaz Gökçe, E., Bilir, S., Öztürkmen, N. D., et al. 2013, First Identification and Absolute Magnitudes of the Red Clump Stars in the Solar Neighbourhood for WISE, NewA, 25, 19

Yong, D., Karakas, A. I., Lambert, D. L., et al. 2008, Heavy Element Abundances in Giant Stars of the Globular Clusters M4 and M5, ApJ, 689, 1031